JOURNAL OF SOLID STATE CHEMISTRY 55, 125–132 (1984)

Defect Structures in $Ba_2Ti_9O_{20}$: Intergrowths with a "Synroc" Hollandite Phase, $BaAl_2Ti_6O_{16}$

A. PRING,* D. A. JEFFERSON, AND J. M. THOMAS

Department of Physical Chemistry, Lensfield Road, Cambridge CB2 1EP, United Kingdom

Received February 23, 1984; in revised form June 4, 1984

High-resolution electron microscopic studies have revealed variations in the length of the tunnel cavities within $Ba_2Ti_9O_{20}$, from the normal cavity of length three sites to ones of four and five sites. These elongated cavities can be described in terms of an intergrowth of distorted synroc hollandite $BaAl_2Ti_6O_{16}$ with $Ba_2Ti_9O_{20}$. The implications of such intergrowths in the immobilization of radioactive cesium are discussed, and a potential homologous series of phases is predicted. © 1984 Academic Press, Inc.

1. Introduction

As an alternative to using borosilicate glass to immobilize high-level radioactive waste, Ringwood *et al.* (*1*) suggested a synthetic rock (synroc) which, unlike the glass, is thermodynamically stable. This material contains three major phases: perovskite, $CaTiO_3$, zirconolite, $CaZrTi_2O_7$, and hollandite, $BaAl_2Ti_6O_{16}$. Use of the latter as the host for radioactive cesium has stimulated a variety of structural studies on hollandites (*2–4*).

Owing to the high TiO_2 and Al_2O_3 contents of the synroc and the synroc hollandite in particular, which prevent economical large-scale preparation by sintering, Ringwood (*5*) originally proposed synthesis by hot-pressing at 1200°C and $1 \rightarrow 3$ kb. The unfavourable economics of this process have prompted a search for a low pressure synthetic route, but attempts in this laboratory to prepare the $BaAl_2Ti_6O_{16}$ hollandite by sintering at 1200°C under atmospheric pressure produced instead barium–titanium oxide, subsequently identified as $Ba_2Ti_9O_{20}$, which has a hollandite-related structure (see below). High-resolution electron microscopic (HREM) images of this material revealed several distinct types of crystallographic defects, and one of these, equivalent to an intergrowth of $Ba_2Ti_9O_{20}$ and $BaAl_2Ti_6O_{16}$, is discussed in detail below.

2. The structure of $Ba_2Ti_9O_{20}$

The phase $Ba_2Ti_9O_{20}$ was first identified by Jonker and Kwestroo (*6*), the stoichiometry being confirmed by Negas *et al.* (*7*). The physical properties of the material, which is a microwave resonator, have been extensively studied (*8*), but the structure has only recently been solved, and related to that of hollandite, using HREM and single-crystal X-ray diffraction methods (*9, 10*). Tillman *et al.* (*11*) also reported a recent X-ray structure determination of $Ba_2Ti_9O_{20}$, and compared the result with other known barium–titanium oxides.

The relationships between the hollandite

* Present address: South Australian Museum, North Terrace, Adelaide, South Australia.

0022-4596/84 $3.00
Copyright © 1984 by Academic Press, Inc.
All rights of reproduction in any form reserved.

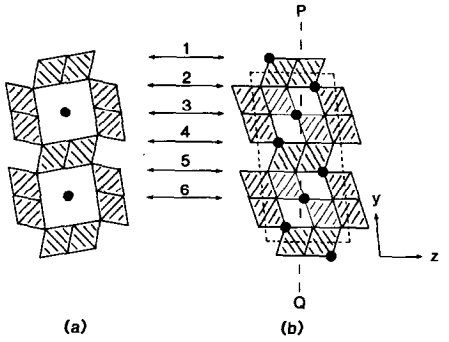

FIG. 1. (a) Schematic projection of the hollandite structure down [001]. Edge-sharing pairs of MO_6 octahedra share corners producing square tunnels occupied by large cations such as Ba^{2+}. (b) The corresponding projection ([100]) in $Ba_2Ti_9O_{20}$. Note the diagonally placed octahedra (in lighter outline) which block the tunnels. The close-packed planes are numbered and Ba^{2+} ions are indicated by filled circles.

and $Ba_2Ti_9O_{20}$ structures are illustrated in Fig. 1. Both structures are composed of tunnels, formed by columns of edge-sharing MO_6 octahedra linked to one another by corner-sharing. In hollandite, large cations such as barium or potassium occupy sites within the tunnels, such sites having approximately cubic symmetry (*12*) and the overall structural arrangement has either tetragonal or monoclinic symmetry (*13*). In $Ba_2Ti_9O_{20}$ however, the structure is heavily distorted, such that the layers of O^{2-} anions are approximately close-packed, and the tunnels are disrupted by blocks of four octahedra which share edges in the direction of the tunnels and corners diagonally across them. The unit cell (a = 14.358 Å, b = 14.095 Å, c = 7.77 Å, α = 95.53°, β = 100.55°, γ = 89.95°) contains six close-packed layers of O^{2-} anions, although polytypic modifications have been reported (*9*) and were also observed in this study. The octahedral blocks which bridge the tunnels are separated by three hollandite-like sites, of which only two are occupied, such that the cation sequence is Ba^{2+}–□–Ba^{2+}, and further Ba^{2+} ions replace oxygen in the

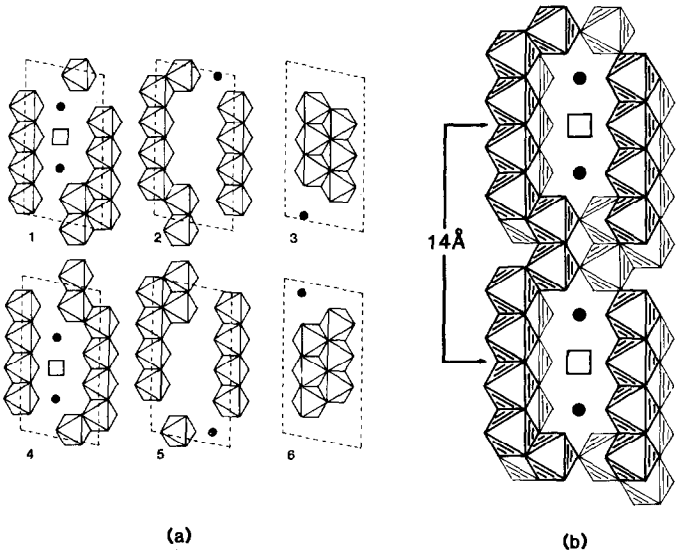

FIG. 2. (a) The (010) sections of the $Ba_2Ti_9O_{20}$ structure, corresponding to each of the numbered close-packed planes indicated in Fig. 1b, these planes constituting the upper surface of the octahedral arrangement shown. Ba^{2+} ions are indicated by filled circles and tunnel site "vacancies" by squares. (b) Perspective view of the tunnels in $Ba_2Ti_9O_{20}$, showing the Ba^{2+}–□–Ba^{2+} repeat and 14-Å vacancy separation. For clarity, Ba^{2+} ions within the framework and upper and lower tunnel walls have been outlined.

framework of the structure at the level of the octahedral blocks. The exact arrangement of the Ba^{2+} ions and TiO_6 octahedra is shown in Fig. 2a, where these are projected onto the close-packed planes of O^{2-} indicated in Fig. 1. The separation of vacancies along the direction equivalent to the hollandite-like tunnels is some 14 Å, and is shown in Fig. 2b. The distortion of the octahedral framework in $Ba_2Ti_9O_{20}$, coupled with an overall increase in the unit cell size over that of hollandite, reduces the symmetry to triclinic.

3. Experimental

$Ba_2Ti_9O_{20}$ was initially prepared during attempts to synthesize $BaAl_2Ti_6O_{16}$ but was subsequently produced by direct sintering of stoichiometric mixtures of BaO and TiO_2 at 1250°C in platinum capsules for periods of up to 14 days. Initial characterization was by X-ray powder diffractometry, using the data of O'Bryan *et al.* (*14*) as a standard. No cell parameter refinement was attempted.

Specimens for HREM studies were prepared by grinding in acetone suspension and deposition onto holey carbon films. Images were recorded at magnifications in the range 300,000–450,000×. Selected area electron diffraction patterns from regions of interest were also recorded, and astigmatism was corrected by observing the granularity of the carbon support film, after precise alignment to achieve axial illumination conditions. The JEM-200CX instrument employed was operated at 200 kV, and was of modified side-entry configuration, with a 45° double-tilt holder working in a high-resolution pole-piece with electron optical characteristics $C_s = C_c = 1.9$ mm. The point resolution of this configuration was ca. 2.7 Å at an optimum defocus of −850 Å, slightly below the so-called Scherzer condition. Image simulations were carried out using the multislice method (*15*) with programs written by one of us (DAJ).

4. Results

HREM investigation of $BaAl_2Ti_6O_{16}$ preparations with relatively short annealing periods indicated a wide variety of disordered structures, some of which could be assigned as defective $Ba_2Ti_9O_{20}$. A typical example of the type of microstructure observed is shown in Fig. 3. After more prolonged annealing, however, the materials became more ordered, giving diffraction patterns similar to those reported by Grzinic *et al.* (*9*). Two types of residual defect were observed. The first of these was the nine-layer repeat reported previously, which can be regarded as arising from a different sequence of successive displacements of the blocking octahedra when the hollandite-like tunnels are stacked in the [010] direction. A micrograph of a second type of defect, distinct from the stacking faults, and less commonly observed, is, however, shown in Fig. 4. In this case the electron beam is parallel to [001], and consequently the "tunnels" lie in the plane of the micrograph. Rows of white dots run across the crystal, the row separation being 14 Å, and the defect is outlined in a region where the local spacing of these rows is some 6 Å, terminating with a 3-Å row separation.

Structural analysis of this defect was achieved by image-matching studies. Computer simulation of images of perfect structural regions confirmed that the rows of white dots were approximately perpendicular to the "tunnels" in the structure and established the imaging conditions of crystal thickness, $\Delta H = 50$ Å, and objective lens defocus, $\Delta f = -950$ Å. As this was close to the optimum focus position, the projected charge density approximation (*16*) was utilized in a preliminary attempt to interpret the image of the defect region. As

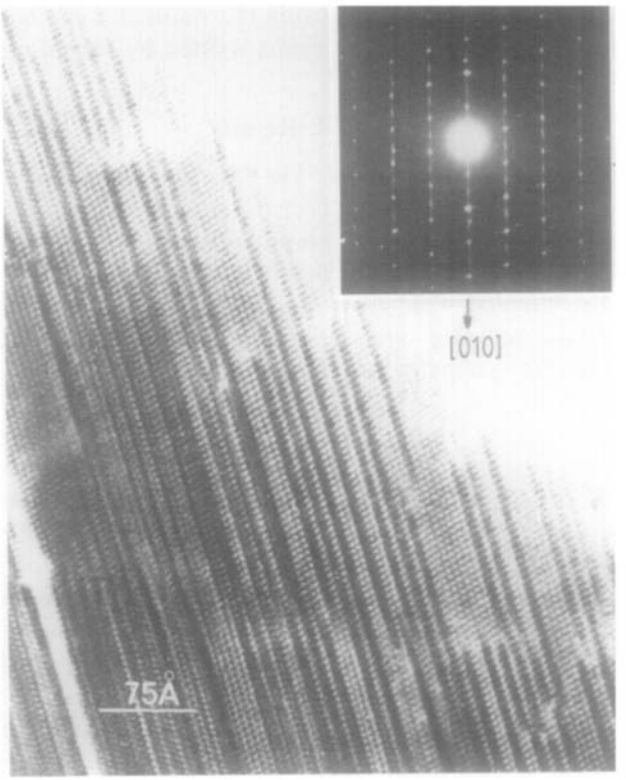

FIG. 3. HREM image of a highly disordered Ba–Al–Ti–O phase after only brief annealing. The electron beam is parallel to [10$\bar{1}$] in the $Ba_2Ti_9O_{20}$ structure. The electron diffraction pattern (inset) shows only diffuse reflections of the 14-Å structure.

the regions of low electron density appeared as white dots, these dots in the image corresponded to the vacant tunnel sites in the $Ba_2Ti_9O_{20}$ structure. In the perfect structure the normal separation of vacant sites along the tunnel axis was ca. 14 Å, and consequently in the defect region, analogous interpretation suggested a separation of vacant tunnel sites of some 6 Å. This corresponds to lengthening the tunnel by two octahedra, and replacing the vacant site in $Ba_2Ti_9O_{20}$ by three sites, two vacancies separated by a further filled site, so that the sequency along the strip of tunnel is now Ba^{2+}–□–Ba^{2+}–□–Ba^{2+}. Figure 5a shows a schematic outline of the local repeat so produced, projected onto the same close-packed planes as in Fig. 2a. The parameters for this defect cell are a = 20.16 Å, b = 14.10 Å, c = 7.50 Å, α = 95.5°, β = 100.5°, γ = 89.9°, with the 20-Å repeat being in the direction of the tunnels. The overall vacancy repeat in this direction is shown in Fig. 5b, together with the 6-Å local separation. The composition of the two octahedra strip inserted into the $Ba_2Ti_9O_{20}$ cell is $Ba_2Ti_{16}O_{32}^{4+}$. To preserve electrical neutrality, substitution of Ti^{4+} by Al^{3+} is necessary, unless reduction of Ti^{4+} occurs (the defects were only observed in Al-containing preparations) and the probable stoichiometrty is $Ba_2Ti_{12}Al_4O_{32}$. A computer-simulated image was produced from this defect, image simulation is shown in inset of Fig. 4.

Using identical reasoning, the short re-

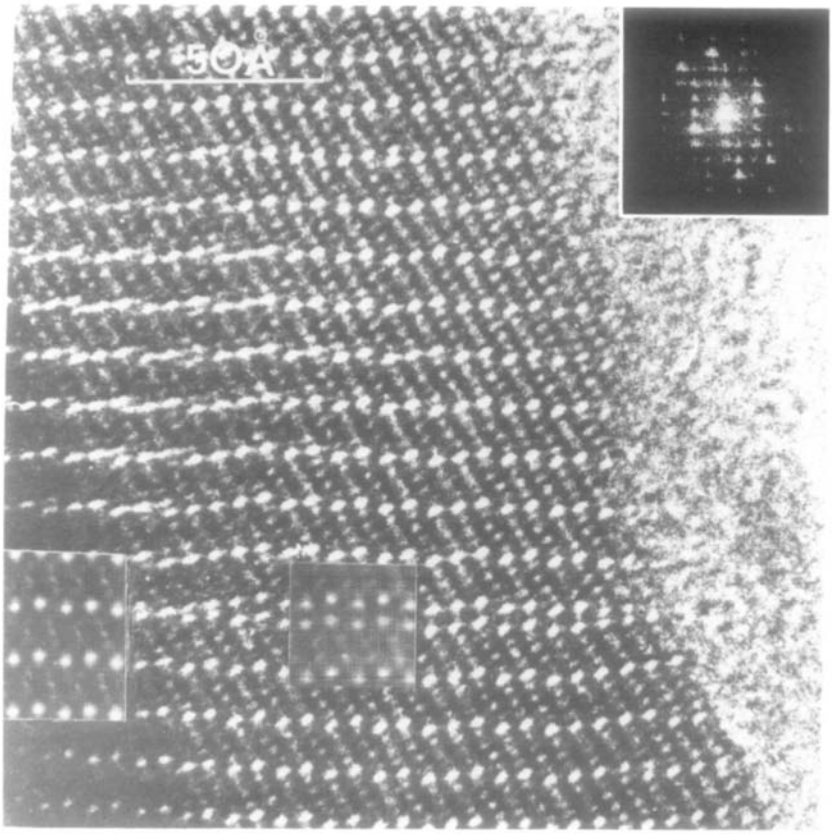

FIG. 4. HREM image of annealed $Ba_2Ti_9O_{20}$ down [001], showing a 6-Å tunnel defect, with (inset) the corresponding optical diffraction pattern from the area of the micrograph. Image simulations are shown inset for both perfect structure and the defect region. Estimated values of crystal thickness and objective lens defocus were 50 and −950 Å, respectively.

gion with a 3-Å separation of the rows of white dots can be interpreted as areas where the tunnel is lengthened only by one octahedron and two vacant tunnel sites occur side-by-side. These defect strips would have the stoichiometry Ti_8O_{16} and require no Al^{3+} substitution. In the example illustrated, the presence of tunnels lengthened by only one octahedron arises from the fact that the 6-Å defect strip does not extend across the full width of the crystal, but grows out before reaching the crystal edge. No effects due to strain and distortion are visible in the image of Fig. 4, and this can be reconciled with the determined structure if the local arrangement is plotted down the [001] axis, as indicated in Fig. 6a. This illustrates how a single strip of the elongated tunnels can be removed, involving two tunnels with adjacent vacancies and a local change in the stacking sequence of blacking octahedra in the [010] direction, producing, in effect, two unit cells of the 21-Å polytype. Figure 6b shows the close correspondence between the vacancy sites and the white dots in the image.

The existence of such defects in $Ba_2Ti_9O_{20}$, and the apparent adaptability of the structural arrangement to varying tunnel length, point to the possibility of a wider

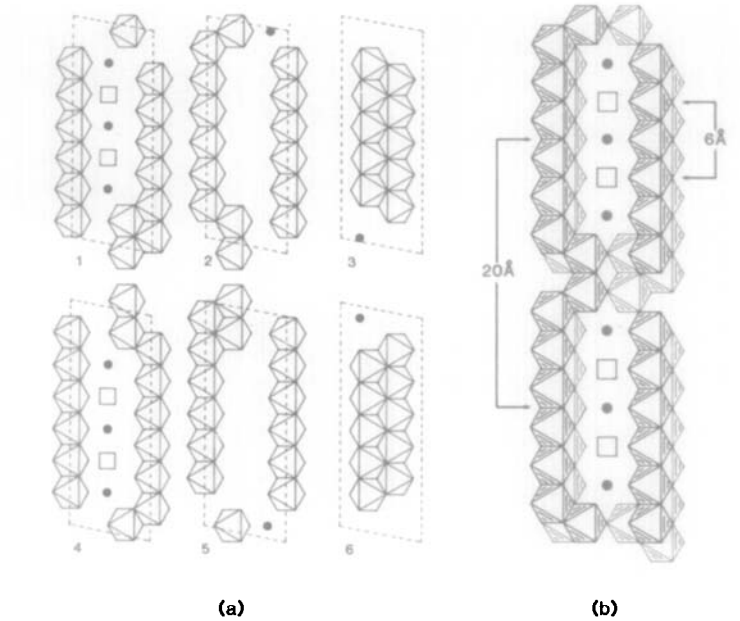

FIG. 5. (a) Structural diagram of the structure in the defect of Fig. 4, projected onto the same close-packed planes of O^{2-} anions. (b) Schematic view of the new, elongated tunnel, showing the overall repeat distance and the 6-Å vacancy separation. Representation of Ba^{2+} and vacancies is the same as that in Fig. 2.

variation in the stoichiometry of this material than was hitherto suspected.

5. Discussion

The defect structures described above suggest that some degree of solid solubility between $Ba_2Ti_9O_{20}$ and the hollandite phase $BiAl_2Ti_6O_{16}$ may be possible, particularly at higher pressures of formation. The tunnel cavities in $Ba_2Ti_9O_{20}$ could be lengthened merely by adding extra octahedra within the tunnel walls, thereby altering the Ba : Ti ratio, but Bystrom and Bystrom (*12*) have demonstrated that the presence of large cations within the tunnels is essential to stabilize the framework. Consequently, incorporation of extra tunnel cations is necessary and this in turn necessitates the substitution of Ti^{4+} by ions of lower valency (such as Al^{3+}) to maintain electrical neutrality. The defect structure discussed above can therefore be regarded as the first member of a hypothetical homologous series with the general stoichiometry $Ba_8Ti_{36}O_{80} + nBaAl_2Ti_6O_{16}$, where $n + 3$ is the length of the tunnel cavity in terms of MO_6 octahedra. This assumes a regular alternation of filled and vacant sites within the tunnels. For large n values, however, one would expect behavior more like the hollandite materials, with additional substitution of Ti^{4+} by Al^{3+} permitting higher Ba contents and consequently giving rise to certain ordering schemes as found in synroc-related hollandites (*2*). Combinations of different tunnel lengths, involving repeated terminations of 6-Å-type defects, might also be possible.

6. Conclusions

In $Ba_2Ti_9O_{20}$ barium ions are trapped either in the framework or within the tunnel cavities. Although the latter can apparently move within the cavities, more extensive movement is prevented by the diagonally

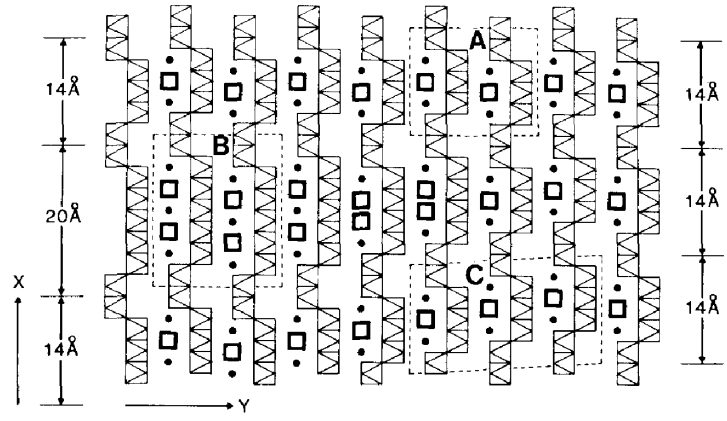

(a)

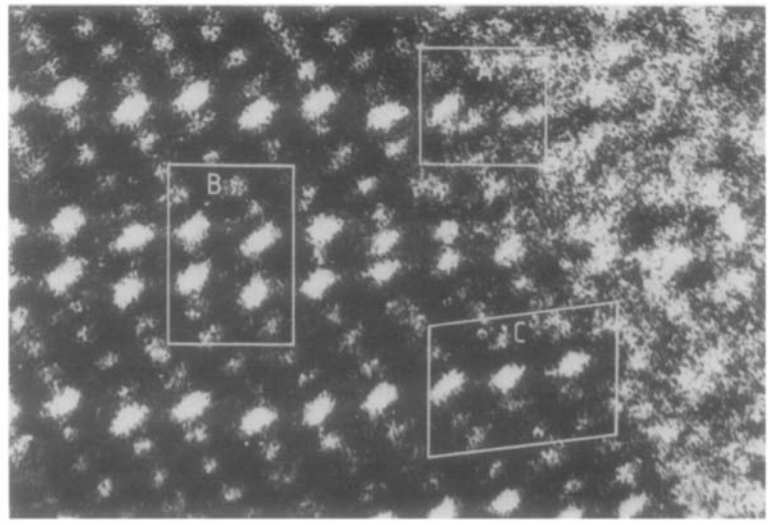

(b)

FIG. 6. (a) The [001] projection of the right-hand part of the defect strip of Fig. 4, indicating how the defect strip alters into the normal $Ba_2Ti_9O_{20}$ structure. The plane of projection is equivalent to PQ in Fig. 1b. The unit meshes A, B, C, correspond to the normal $Ba_2Ti_9O_{20}$ structure, the structure with elongated tunnels, and the 21-Å polytype phase, respectively. (b) The corresponding portion of the image, with the white dots indicating the tunnel site vacancies. Octahedral distortion produces a larger-than-ideal repeat along the tunnel axis.

placed blocks of octahedra. The leaching resistance of $Ba_2Ti_9O_{20}$ might therefore be expected to be as good as, if not better than the synroc hollandite and the introduction of longer tunnel cavities by incorporating defects of the type described above should not affect this property, but could even assist in the substitution of caesium for barium within the cavities. A regular intergrowth structure of this type would therefore have all the advantages of a synroc hollandite but could also be prepared without the need for hot-pressing.

Clearly, further studies of the system

$Ba_2Ti_9O_{20}$–$BaAlTi_6O_{16}$ are required. The extent to which Al^{3+} enters the structure must be established, as this will clearly determine the length of the tunnel cavities. Further experimental studies to establish the stability fields (if any) of the intergrowth structures is also necessary. The extent to which Cs^+ can substitute for Ba^{2+} is also being investigated.

Acknowledgments

The support of A. E. R. E. Harwell, the University of Cambridge, and the SERC is gratefully acknowledged. We are grateful to Dr. B. M. Gatehouse and Dr. L. A. Bursill for making available their results and for helpful discussions.

References

1. A. E. Ringwood, S. E. Kesson, N. G. Ware, W. Hiberson, and A. Major, *Geochem. J.* **13,** 141 (1979).
2. L. A. Bursill and G. Grzinic, *Acta Crystallogr. Sect. B* **36,** 2902 (1980).
3. W. Sinclair, G. M. McLaughlin, and A. E. Ringwood, *Acta Crystallogr. Sect. B* **36,** 2913 (1980).
4. H. U. Beyeler and C. Schuller, *Solid State Ionics* **1,** 77 (1980).
5. A. E. Ringwood, "Safe Disposal of High Level Nuclear Reactor Wastes. A New Strategy," A.N.U. Press, Canberra (1978).
6. G. H. Jonker and W. Kwestroo, *J. Amer. Ceram. Soc.* **41,** 390 (1958).
7. T. Negas, R. S. Roth, H. S. Parker, and D. Minor, *J. Solid State Chem.* **9,** 297 (1974).
8. J. K. Plourde, D. F. Linn, H. M. O'Bryan, and J. Thomson, *J. Amer. Ceram. Soc.* **58,** 418 (1975).
9. G. Grzinic, L. A. Bursill, and D. J. Smith, *J. Solid State Chem.* **47,** 151 (1983).
10. G. D. Fallon and B. M. Gatehouse, *J. Solid State Chem.* **49,** 59 (1983).
11. E. Tillman, W. Hofmeister, and W. H. Baur, *J. Amer. Ceram. Soc.* **66,** 268 (1983).
12. A. Bystrom and A. M. Bystrom, *Acta Crystallogr.* **3,** 146 (1950).
13. M. C. Cadee and G. C. Verschoor, *Acta Crystallogr Sect. B* **34,** 3554 (1978).
14. H. M. O'Bryan, J. Thomson, and J. K. Plurde, *J. Amer. Ceram. Soc.* **57,** 280 (1974).
15. P. Goodman and A. F. Moodie, *Acta Crystallogr. A* **30,** 280 (1974).
16. D. F. Lynch, A. F. Moodie, and M. A. O'Keefe, *Acta Crystallogr. A* **31,** 300 (1975).